



1 **Transported aerosols regulate the pre-monsoon atmosphere over North-East India: a**
2 **WRF-Chem modelling study**

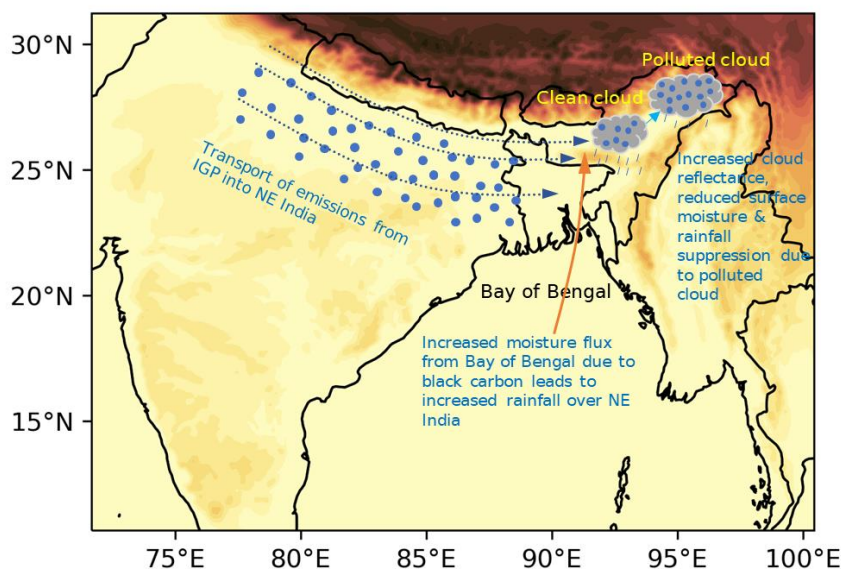
3 Neeldip Barman¹, Sharad Gokhale²

4 ¹Department of Civil Engineering, Indian Institute of Technology Guwahati, Guwahati, 781039, India

5 ²Department of Civil Engineering, Indian Institute of Technology Guwahati, Guwahati, 781039, India

6 *Correspondence to:* Sharad Gokhale (sharadbg@iitg.ac.in)

7 **Abstract.** The study differentiates and quantifies the impacts of aerosols emitted locally within North-East (NE)
8 India region and those transported from outside this region to ascertain whether local or transported aerosols are
9 more impactful in influencing this region's atmosphere during the pre-monsoon season (March-April-May). Due
10 to the existence of a declining pre-monsoon rainfall trend in NE India, the study also quantified the role of different
11 aerosol effects w.r.t radiative forcing (RF) and rainfall. The study has been carried out using the WRF-Chem
12 model by comparing simulation scenarios where emissions were turned on and off within and outside the NE
13 region. The impact of all emissions as a whole and Black carbon (BC) specifically was studied. Results show that
14 aerosols transported primarily from the Indo-Gangetic Plain (IGP) were responsible for 93.98 % of the PM₁₀ mass
15 over NE India's atmosphere and 64.18 % of near-surface PM₁₀ concentration. Transported aerosols contributed
16 >50 % of BC, organic carbon, sulfate, nitrate, ammonium and dust aerosol concentration and hence a major
17 contributor to air pollution. Hence, the aerosol effects were observed to be much greater with transported aerosols.
18 Indirect aerosol effect was found to be the major effect and more impactful with transported aerosols that
19 dominated both rainfall and RF, and suppressed rainfall significantly than the direct and semi-direct effect.
20 However, the increase in direct radiative effects with an increase in transported BC counteracted the rainfall
21 suppression caused by relevant processes of other aerosol effects. Thus, this study shows atmospheric transport
22 to be an important process for this region as transported emissions, specifically from IGP were also found to have
23 greater control over the region's rainfall. Thus, emission control policies implemented in IGP will reduce air
24 pollution as well as the climatic impacts of aerosols over the NE India region.



25

26 1 Introduction

27 Aerosols regulate the Earth's energy budget and hydrological cycle through scattering and absorption of solar
28 radiation and acting as sites for the formation of cloud droplets, which leads to its varied effects, viz. direct, semi-
29 direct and indirect effects (Mitchell, 1971; Rosenfeld, 2012; Menon et al., 2002). The effects differ spatially
30 depending on the constituents of aerosols, their physical and chemical properties as well as the quantity. Among
31 these factors, atmospheric transport also plays an important role which extends the climatic impacts to the
32 transported region from the source region (Lee et al., 2022). The IGP is a global hotspot of diverse aerosols (Ojha
33 et al., 2020; Kumar et al., 2018) that impacts regional and global climate (Ramanathan et al., 2005; Tripathi et al.,
34 2005; Sarangi et al., 2015). Air masses transport aerosols from the IGP to nearby regions, which also impact air
35 quality (Bhat et al., 2022; Ojha et al., 2012). Bonasoni et al. (2010) showed that pollutants from the IGP follow
36 the southern slope of the Himalayas as a path into the Bay of Bengal and NE India and similar observations were
37 made by Gogoi et al. (2017). The condition becomes more critical in the pre-monsoon season when the westerlies
38 directly transport air pollutants from the IGP to NE India. Among the aerosols, BC is a high climate-influencing
39 aerosol component due to its strong absorption capability (Bond et al., 2013; Nenes et al., 2002; Koch and Del
40 Genio, 2010) and IGP is the largest source region of it in India (Rana et al., 2019). Several studies (Guha et al.,
41 2015; Sarkar et al., 2019; Chatterjee et al., 2010) found BC, among other aerosols measured at sites in NE India
42 to be transported from the IGP. Moreover, in the NE India region, an increase in BC emissions was observed
43 along with high BC concentrations near the surface level (Barman and Gokhale, 2019; Chaudhury et al., 2022;
44 Singh and Gokhale, 2021). Tiwari et al. (2016) observed maximum BC concentration during this season in this
45 region along with the highest surface RF. The region also observes the highest atmospheric heating and highest
46 aerosol optical depth with an increasing trend during this period (Nair et al., 2017; Dahutia et al., 2018; Dahutia
47 et al., 2019; Gogoi et al., 2017; Pathak et al., 2010; Pathak et al., 2016). The presence of high aerosol loading



48 along with high atmospheric heating is likely to have varied aerosol effects over the region and may also have an
49 important role to play with the rainfall. Mondal et al. (2018) showed a decreasing trend of pre-monsoon rainfall
50 in this biodiversity hotspot region. Few modelling studies (Kant et al., 2021; Kedia et al., 2016; Kedia et al., 2019)
51 are available that studied the aerosol effect on rainfall over India. However, only Soni et al. (2017) and Barman
52 and Gokhale (2022) studied the BC effect on pre-monsoon rainfall in this region but without the inclusion of
53 aerosol indirect effect. Both studies found BC to increase total rainfall but Barman and Gokhale (2022) also found
54 semi-direct effect to be a rainfall suppression mechanism by evaporating clouds between 1 to 2 km above ground
55 level.

56 However, a few questions remained to be answered. How much is the contribution of transported aerosols
57 to air pollution and climatic effects compared to those emitted within NE India region? What is the role of different
58 aerosol effects on the rainfall mechanisms? Thus, this study was carried out with the following objectives (a)
59 Compare the contributions of local and transported aerosols to air pollution and different climatic effects over NE
60 India (b) Quantify the role of different aerosol effects on the climatic effects (c) Investigate the role of BC emitted
61 within NE India and transported BC in such climatic effects. Here, transported aerosols include the transported
62 primary aerosols emitted from outside NE India as well as the secondary aerosols formed from the transported
63 emissions. Same goes for local emissions. Through qualitative and quantitative comparison of the impacts of local
64 and transported aerosols, the study tries to find the source region of aerosols that has a greater impact on the
65 atmosphere over NE India during the pre-monsoon season. Since observational studies cannot distinguish between
66 the local and transported aerosols impacts, the study was carried out with numerical modelling. The effect of
67 transported aerosols on different regions of the world has been studied (Krishnamohan et al., 2021; Wang et al.,
68 2020; Bagtasa et al., 2019) but none of them covered the IGP and its impact on the nearby region.

69 2 Methods

70 The study used the WRF-Chem v4.2.1 model (Grell et al., 2005). The model configuration, modelling domain,
71 model inputs and simulation period is similar to the one used in Barman and Gokhale (2022) and details regarding
72 the same is provided in that study. The model was run for a duration of 13 days from 7-19 April 2018, out of
73 which a 3-day period from 7-9 April 2018 was discarded as spin-up and outputs from 10-19 were used for analysis.
74 The period represents the mid of pre-monsoon season. Also, April 2018 was Indian Ocean Dipole and ENSO
75 neutral period and hence suitable for study of aerosol effects. The climatic situation during the study period was
76 also described in Barman and Gokhale (2022). The near surface wind flow was from the Bay of Bengal towards
77 NE India, which gradually changed to westerly wind flow carrying aerosols from IGP towards NE India.
78 Descriptions of the simulations are provided in Table 1.

79 Table 1: Description of simulations

	Simulation name	Description of simulations
1.	NOR-I	Baseline simulation with all aerosol effects
2.	NOFEED-I	Same as NOR-I but with aerosol radiative effects turned off
3.	NOCHEM	Simulation with no atmospheric chemistry and aerosol effects
4.	No_EMISS_NE	Same as NOR-I but with emissions turned on only outside NE India
5.	Only_EMISS_NE	Same as NOR-I but with emissions turned on only within NE India



6.	No_EMISS_NE_4SO ₂	Same as No_EMISS_NE but with 4×SO ₂ emissions
7.	No_EMISS_NE_0.25SO ₂	Same as No_EMISS_NE but with 0.25×SO ₂ emissions
8.	No_EMISS_NE_NOFEED	Same as No_EMISS_NE but with aerosol radiative effects turned off
9.	Only_EMISS_NE_NOFEED	Same as Only_EMISS_NE but with aerosol radiative effects turned off
10.	No_NE_BCI	Same as NOR-I but with BC emissions turned on only outside NE India
11.	Only_NE_BCI	Same as NOR-I but with BC emissions turned on only within NE India
12.	4NOR-I	Same as NOR-I but with 4×BC emissions
13.	No_BC_ABS	Same as NOR-I but with BC absorption disabled
14.	NOR	Baseline simulation with only direct and semi-direct effect
15.	2NOR	Same as NOR but with 2×BC emissions
16.	No_NE_BC	Same as NOR but with BC emissions within NE India region turned off
17.	No_NE_2×BC	Same as No_NE_BC but with 2×BC emissions outside NE India
18.	Only_NE_BC	Same as NOR but with BC emissions turned off outside NE India
19.	Only_NE_2×BC	Same as Only_NE_BC but with 2×BC emissions inside NE India
20.	NOFEED	Same as NOR but with aerosol radiative effects off

80

81 All the simulations were conducted with the MOZART-MOSAIC chemistry scheme, except simulation 3, which
 82 was purely a meteorology simulation and did not include any atmospheric chemistry and aerosol effects. As per
 83 Ghan et al. (2012) and Bauer and Menon (2012), the total aerosol effect is the algebraic sum of direct, indirect
 84 and semi-direct effects. Similar approaches were used by Yang et al. (2011). Thus,

$$85 \text{ NOR-I} - \text{NOCHEM} = \text{Total aerosol effect} = \text{Direct} + \text{Semi-direct} + \text{Indirect}, \quad (1)$$

86 Both NOFEED-I and NOR-I includes indirect effect but NOFEED-I does not include aerosol radiative effects.
 87 Thus,

$$88 \text{ NOR-I} - \text{NOFEED-I} = \text{Direct} + \text{Semi-direct effect}, \quad (2)$$

89 Also, since NOFEED-I includes only indirect effect,

$$90 \text{ NOFEED-I} - \text{NOCHEM} = \text{Indirect effect}, \quad (3)$$

91 Similar approaches were used by Wang et al. (2015).

92 No_EMISS_NE had all emissions (biogenic, anthropogenic and dust) disabled within the NE India region
 93 bounded by 22° N and 29° N latitudes and 89° E and 97° E longitudes, shown by the blue box in Fig. 1(a).
 94 Similarly, Only_EMISS_NE had all emissions disabled outside of the above region along with boundary
 95 conditions for all chemical species modified to zero to nullify the transport of emissions from outside the domain.
 96 Simulations 14 to 20 were specifically used to understand the contribution of local and transported BC emissions
 97 as well the response of emission increase on radiative heating, atmospheric dynamics and moisture without the
 98 interference of indirect aerosol effect.

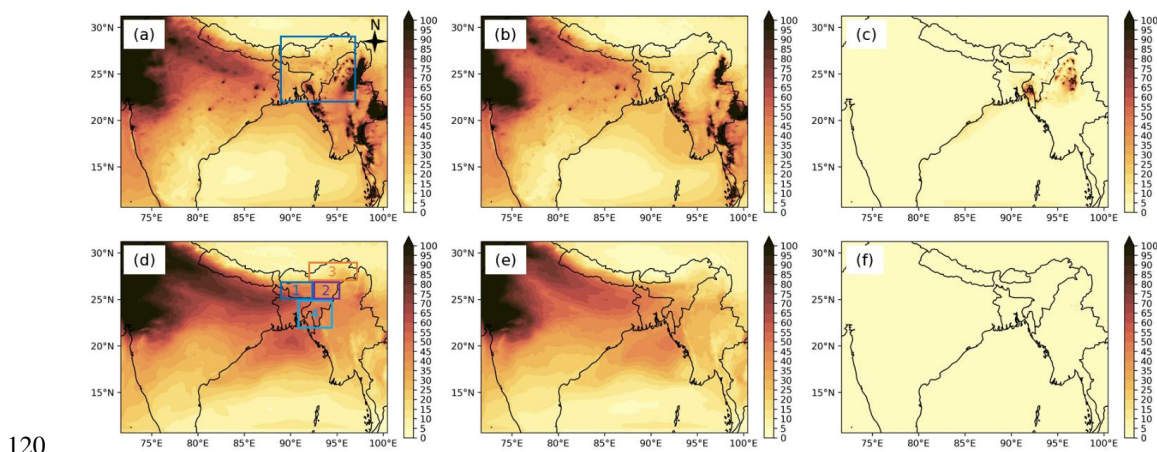
99 The NOR simulation utilised in this study was evaluated in Barman and Gokhale (2022). Moreover,
 100 meteorological evaluation of NOR-I w.r.t wind direction, wind speed, temperature and humidity was carried out



101 against surface station datasets (<https://mesonet.agron.iastate.edu/sites/locate.php>) at Guwahati (26.10 °N, 91.58
102 °E), Kolkata (22.65 °N, 88.45 °E), Bangalore (13.20 °N, 77.70 °E), Patna (25.59 °N, 85.08 °E), Delhi (28.56 °N,
103 77.11 °E) and Mumbai (19.10 °N, 72.86 °E). Simulated rainfall was evaluated against the Indian Meteorological
104 Department (IMD) rainfall dataset of Pai et al. (2014) (https://www.imdpune.gov.in/Clim_Pred_LRF_New/Grided_Data_Download.html). Index of agreement (IOA),
105 root mean square error (RMSE) and mean error (ME) were used as statistical parameters. As per the criteria of
106 Emery et al. (2001), the NOR-I simulation underpredicted temperature but showed good performance with wind
107 speed and wind direction but had large RMSE with wind direction, similar to the NOR simulation. Performance
108 statistics are provided in Table S1. Moreover, NOR and NOR-I simulated chemical species (BC, organic carbon,
109 dust and sulfate aerosol) were compared against the MERRA2 dataset
110 (https://disc.gsfc.nasa.gov/datasets/M2T1NXAER_5.12.4/summary) at the above locations. Performance
111 statistics are shown in Table S2. NOR gave a much better estimation of all the chemical species at all locations.
112 However, the inclusion of all aerosol effects greatly improved simulated rainfall performance with NE India
113 regional average IOA: 0.52, ME: 3.72 mm day⁻¹, RMSE: 13.55 mm day⁻¹ compared to only considering direct +
114 semi-direct effect (IOA: 0.40, ME: 9.22 mm day⁻¹, RMSE: 21.26 mm day⁻¹) in Barman and Gokhale (2022). The
115 improvement in performance and decrease in ME show that indirect effect played a major role during this period
116 in controlling and suppressing rainfall.
117

118 3 Results and discussion

119 3.1 PM₁₀ spatial and atmospheric distribution



120
121 Figure 1: Spatial distribution of PM₁₀ concentration ($\mu\text{g m}^{-3}$) in NOR-I, (a, d), No_EMISS_NE (b, e) and
122 Only_EMISS_NE (c, f). Upper row shows distribution at model level 0 (near surface) and the lower row at model
123 level 15

124 Figure 1 shows the time-averaged spatial distribution of PM₁₀ concentration. The spatial distribution of
125 geopotential heights of model level 0 and 15 are shown in Fig. S1, while region-wise (Fig. 1(d)) concentration
126 values within NE India at the two atmospheric heights are shown in Table S3. PM₁₀ concentration contours shown
127 in Fig. 1(a), 1(b), 1(d) and 1(e), emanating from IGP and spreading into NE India indicated the transport of

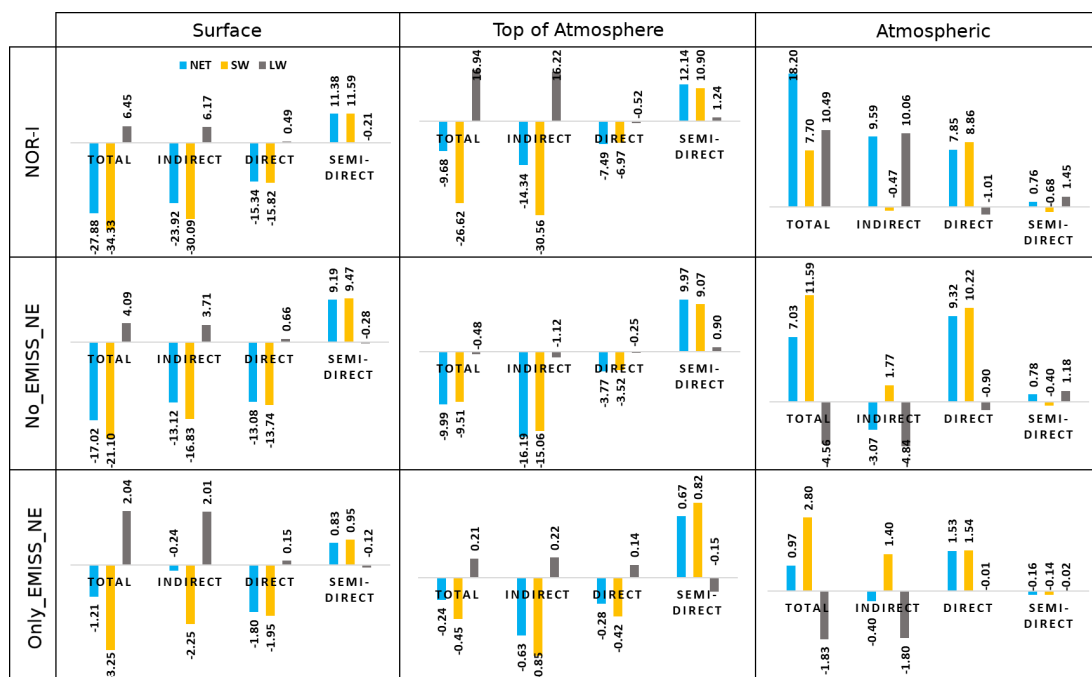


128 aerosols from IGP into NE India. The similarity of these spatial distributions of No_EMITT_NE to the baseline
129 scenario, NOR-I, especially within NE India region inferred that most of the aerosol mass within NE India was
130 contributed by transported aerosols, while PM₁₀ emitted or formed over NE India remained mainly confined
131 within the region as shown in Fig. 1(c), possibly due to the mountainous terrain, as also described in Kundu et al.
132 (2018). Both near the surface and at higher atmosphere (level 15), No_EMITT_NE showed a higher regional
133 average concentration (surface: 14.46 $\mu\text{g m}^{-3}$, higher atmosphere: 24.43 $\mu\text{g m}^{-3}$) which was closer to the baseline
134 scenario of NOR-I (surface: 27.43 $\mu\text{g m}^{-3}$, higher atmosphere: 34.13 $\mu\text{g m}^{-3}$) compared to the local emission
135 scenario of Only_EMITT_NE (surface: 8.07 $\mu\text{g m}^{-3}$, higher atmosphere: 0.98 $\mu\text{g m}^{-3}$). Thus, transported aerosols
136 contributed higher PM₁₀ concentration (64.18 %) than local emission and contribution from local emissions were
137 negligible at higher atmosphere, as also seen in Fig. 1(f) and 96.14 % of it was contributed by transported aerosols.
138 The higher concentration at higher atmosphere was due to transported aerosols developing an elevated PM₁₀
139 profile (Fig. S2) having maximum concentration near 2000 m and which shows much greater similarity with the
140 baseline scenario. The long range transport and strong convective active during this season is responsible for the
141 elevated profile (Pathak et al. (2016)). Hence, transported aerosols contributed to bulk of the aerosols over NE
142 India throughout the atmospheric column (93.98 %) indicated by the column integrated PM₁₀ mass of 313.97 g
143 m⁻² (No_EMITT_NE) and 20.08 g m⁻² (Only_EMITT_NE). NOR-I had column integrated PM₁₀ mass of 466.63 g
144 m⁻². Further analysis indicated that transported aerosols accounted for >50 % of BC, organic carbon, sulfate,
145 nitrate, ammonium and dust aerosol mass over NE India's atmosphere. Regions 1, being in close proximity to
146 IGP, as seen in Fig. 1(c), received maximum near surface aerosol mass (73.70 %) from transported aerosols,
147 compared to the other regions, followed by region 2 (66.86 %), 3 (60.48 %) and 4 (57.43 %). However, even
148 though No_EMITT_NE and Only_EMITT_NE is the bifurcation of NOR-I into two separate emission regions,
149 the sum of No_EMITT_NE and Only_EMITT_NE column integrated mass as well as concentrations didn't equate
150 to NOR-I values and is always less than it. This indicated formation of extra aerosol mass due to interaction of
151 emissions of the two regions.

152 3.2 Aerosol effects of local and transported aerosols on radiative forcing

153 RF due to different aerosol effects was estimated based on the methodology described in Sect. 2. Further details
154 regarding its estimation are provided in the supplementary.

155 The baseline scenario indicated that direct and indirect aerosol effects caused net (NET) surface and top
156 of the atmosphere (TOA) dimming while causing atmospheric heating. This is due to the presence of aerosols that
157 scatter and absorb solar radiation, reducing it at the surface while increasing it at the top of the atmosphere as well
158 as causing atmospheric heating. Net direct surface, TOA and atmospheric RF were -15.34, -7.49 and 7.85 Wm⁻²
159 and was mainly contributed by short-wave (SW) radiation. Indirect effect had the same effect on solar radiation
160 as the direct effect and was due to the formation of numerous smaller cloud droplets which has better reflectivity
161 to solar radiation, also known as the 1st indirect effect or Twomey effect (Twomey, 1977) and However, positive
162 atmospheric RF (18.20 W m⁻²) causing atmospheric heating (10.06 W m⁻²) was mainly caused by long-wave (LW)
163 radiation (16.22 W m⁻²) at the TOA contributed by indirect effect. This was due to greater cloud cover (Fig. S3)
164 at 8 – 10 km which is not seen in the other two scenarios. The indirect effect also caused warming at the surface
165 (6.17 W m⁻²), as its contributed to greater cloud cover (Nandan et al., 2022) causing heating of the surface through
166 LW radiation. The total net surface RF was -27.88 W m⁻² out of which -23.92 W m⁻² or 85.80% was contributed



167

168 Figure 2: NE India regional average RF ($W m^{-2}$) due to different aerosol effects at NET, SW and LW wavelengths
 169 in different emission scenarios

170 by indirect forcing. Indirect SW forcing ($-30.08 W m^{-2}$) was almost twice the direct SW forcing ($-15.82 W m^{-2}$),
 171 while semi-direct SW forcing ($+11.58 W m^{-2}$) was $\sim 75\%$ of the direct forcing. Semi-direct effect showed positive
 172 surface RF due to cloud cover reduction. Thus, atmospheric heating and the subsequent evaporation of clouds
 173 compensated to a large extent the reduction in solar radiation due to aerosols. The atmospheric RF ($0.76 W m^{-2}$)
 174 due to semi-direct effect was due to LW radiation, which may be due to increased solar radiation at the surface,
 175 which released the heat into the atmosphere in the form of LW radiation. However, this value was very small. The
 176 indirect RF contributed most to the total surface, TOA and atmospheric RF at both SW and LW wavelengths and
 177 hence was found to be the dominant aerosol effect affecting radiation over NE India.

178 Quantitatively, No_EMISS_NE provided RF values (surface: $-17.02 W m^{-2}$, TOA: $-9.99 W m^{-2}$ and
 179 atmospheric RF: $7.03 W m^{-2}$) that were much similar and closer to the baseline scenario (surface: $-27.88 W m^{-2}$,
 180 TOA: $-9.68 W m^{-2}$ and atmospheric RF: $18.20 W m^{-2}$) than Only_EMISS_NE (surface: $-1.21 W m^{-2}$, TOA: -0.24
 181 $W m^{-2}$ and atmospheric RF: $0.97 W m^{-2}$). Consequently, the No_EMISS_NE net indirect, direct and semi-direct
 182 surface RF values of -13.12 , -13.08 and $9.19 W m^{-2}$ were significantly larger than the corresponding
 183 Only_EMISS_NE RF values of -0.24 , -1.80 and $0.83 W m^{-2}$. A similar conclusion could be inferred at TOA also.
 184 Hence transported aerosols were primarily responsible for all the different aerosol effects on radiation over NE
 185 India as a greater amount of aerosol mass was contributed by it. Moreover, No_EMISS_NE net direct atmospheric
 186 RF ($9.32 W m^{-2}$) was found to be even higher than the baseline scenario ($7.85 W m^{-2}$). This indicated that the NE
 187 India region contained more scattering aerosols while transported aerosols contained more absorbing aerosols as



188 the difference in the direct atmospheric RF is mainly driven by changes in the TOA RF (-7.49 vs. -3.77 W m⁻²)
189 than surface RF (-15.34 vs. -13.08 W m⁻²). Region 1 had the highest direct and semi-direct net surface RF of -
190 20.41 W m⁻² and 19.20 W m⁻², respectively due to its close proximity to IGP.

191 3.3 Aerosol effects of local and transported aerosols on rainfall

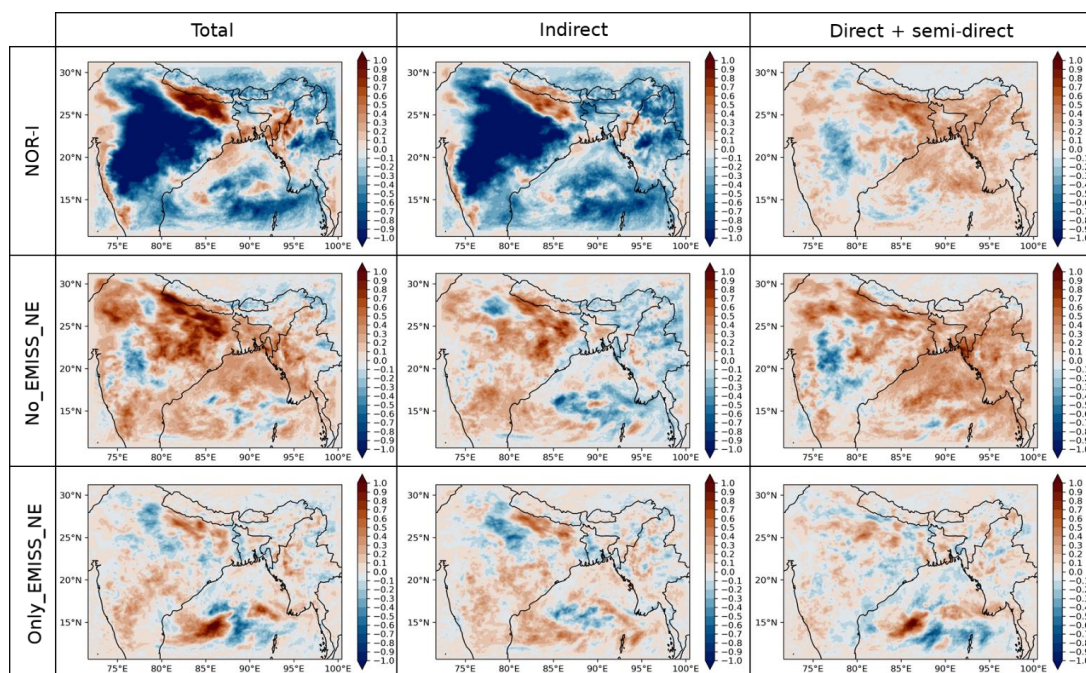
192 Table 2: Changes in rainfall due to different aerosol effects in different scenarios (mm)

	Total aerosol effect	Direct + semi-direct	Indirect
NOR-I	-275.13	-17.04	-258.09
No_EMISS_NE	-73.06	-23.95	-49.11 ⁴
Only_EMISS_NE	-24.45	-8.42	-16.04 ¹⁹⁵

196 The quantitative changes in regional average rainfall amounts over NE India due to the different aerosol effects
197 induced by the aerosols in different scenarios are provided in Table 2. Region-wise values can be read from Table
198 S4. Rainfall from region 4 was not considered due to large errors being associated with it (Fig. S4). In the baseline
199 scenario (NOR-I), the total aerosol effect caused rainfall suppression in all three regions, with a regional total of
200 -275.13 mm, shown in Table 2. Reductions in rainfall due to the total aerosol effect was contributed by
201 suppressions due to both direct + semi-direct and indirect effect and was observed in all the considered regions.
202 The highest suppression was observed in region 3 (-102.60 mm), followed by region 1 (-100.60 mm). The role of
203 direct + semi-direct effect was observed to be minimal with a total regional suppression of -17.04 mm while the
204 indirect effect (-258.09 mm) was responsible for almost the whole of the suppression of -275.13 mm. Region 1
205 observed the highest suppression of -13.21 mm due to direct + semi-direct effect as this region's radiation was
206 highest impacted by these effects.

207 Direct effect could suppress rainfall by reducing surface evaporation and convection through surface
208 dimming while semi-direct by evaporation of clouds (Talukdar et al., 2019; Lohmann and Feichter, 2001; Habib
209 et al., 2006; Bollasina et al., 2011; Koch and Del Genio, 2010b). However, the surface dimming by indirect effect
210 (-23.92 W m⁻²) with NOR-I was much larger than the combined direct + semi-direct effect (-3.96 W m⁻²). Hence
211 the reduction in surface moisture flux due to indirect effect (-6.45×10⁻⁶ kg m⁻² s⁻¹) was much greater than due to
212 combined direct + semi-direct effect (-1.1×10⁻⁶ kg m⁻² s⁻¹) and much similar to the reduction due to total aerosol
213 effect (-7.56×10⁻⁶ kg m⁻² s⁻¹). This was also observed in the case of No_EMISS_NE. The greater surface dimming
214 of -17.02 W m⁻² in No_EMISS_NE caused a much higher negative surface moisture flux change of -3.82×10⁻⁶ kg
215 m⁻² s⁻¹ due to total aerosol effect, mostly contributed by indirect effect (-2.79×10⁻⁶ kg m⁻² s⁻¹) compared to direct
216 + semi-direct effect (-1.03×10⁻⁶ kg m⁻² s⁻¹). Hence, indirect effect in NOR-I and No_EMISS_NE dominated
217 moisture reduction through reduction in surface moisture flux over most areas of NE India at both low and high-
218 terrain regions, as seen in Fig. 3.

219 However, direct + semi-direct effect caused an increase of moisture in NOR-I and No_EMISS_NE over
220 most of NE India in spite of a negative surface moisture flux not observed in Only_EMISS_NE. This indicated
221 that direct + semi-direct caused an increase in the transport of moisture from another region, in this case from Bay
222 of Bengal. The equivalent potential temperature (EPT) profiles in Fig. 4 compare the atmospheric stability due to



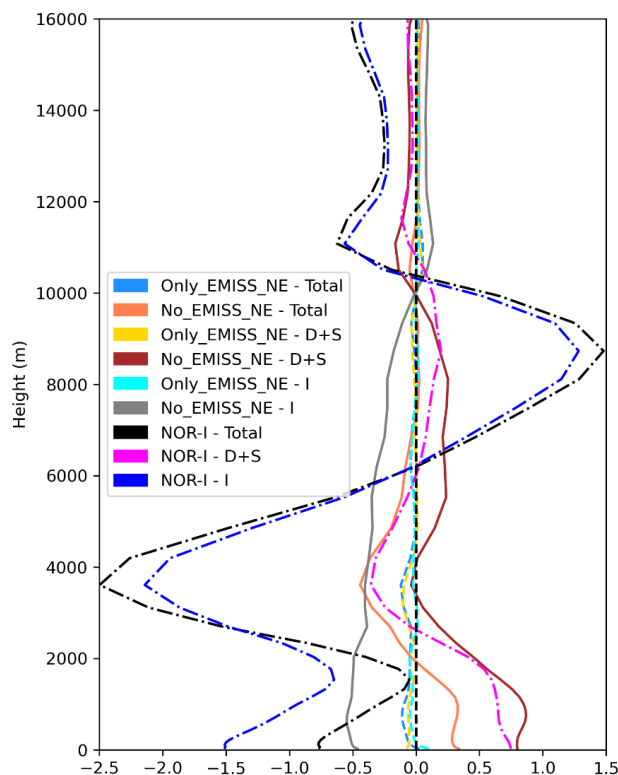
223

224 Figure 3: Spatial distribution of change in near-surface water vapor mixing ratio (g kg^{-1}) due to total aerosol effect,
 225 direct + semi-direct effect and indirect effect

226 different aerosol effects. The greater surface dimming due to the indirect effect in No_EMISS_NE caused not
 227 only negative surface moisture flux but also a significant increase in atmospheric stability (indicated by increasing
 228 value of indirect effect EPT profile with height), reducing convection, which possibly also contributed reduction
 229 to rainfall suppression. However, although the direct + semi-direct EPT profile showed increased atmospheric
 230 stability below 1 km, but created an overall unstable atmosphere in the lower atmosphere. This instability,
 231 primarily caused due to atmospheric heating of BC, created an unstable region over NE India which facilitated
 232 the increased transport of moisture from the Bay of Bengal (discussed later). Hence, though the direct effect
 233 reduces rainfall by reducing surface moisture flux and convection but also possibly enhances it by transporting
 234 moisture. This transported moisture possibly compensated to some extent the rainfall reduction due to a decrease
 235 in surface moisture flux, convection and cloud evaporation caused by direct and semi-direct effects. Hence, the
 236 rainfall reduction due to direct + semi-direct effect (-17.04 mm) was possibly significantly less than the indirect
 237 effect (-258.09 mm). Thus, the effect of direct and indirect effects on dynamics was distinctly different. The EPT
 238 profile of the total aerosol effect in No_EMISS_NE showed an unstable lower atmosphere, supporting moisture
 239 transport. Similar explanation could be given for moisture increase due to direct + semi-direct in NOR-I but the
 240 increase in atmospheric stability and moisture reduction due to greater surface dimming by its indirect effect was
 241 significantly larger, which created an overall stable atmosphere due to total aerosol effect in NOR-I. The EPT
 242 profiles of Only_EMISS_NE showed almost zero perturbation throughout the atmosphere and hence was unable
 243 to affect atmospheric stability and cause moisture transport. Thus, the direct + semi-direct effect in
 244 Only_EMISS_NE did not show significant moisture change in Fig. 3. Moreover, the significantly smaller surface
 245 dimming (-1.21 W m^{-2}) in Only_EMISS_NE caused very small but positive change of $8.15 \times 10^{-8} \text{ kg m}^{-2} \text{ s}^{-1}$ due to



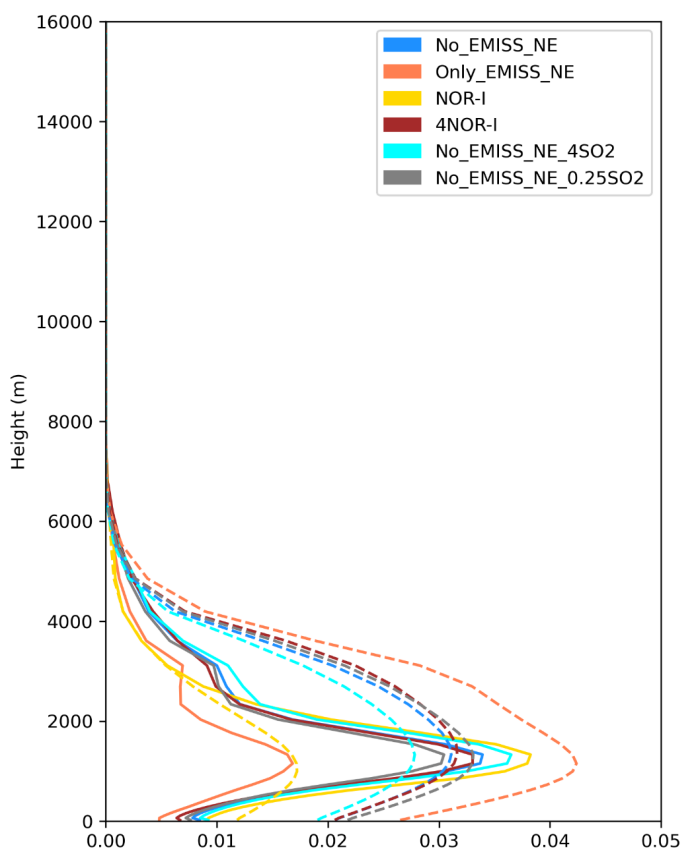
246 the total aerosol effect and hence similar moisture change is observed in Fig. 3. Hence aerosols emitted solely
247 from NE India had negligible capability in affecting moisture through different aerosol effects. Moisture reduction
248 over NE India was much greater due to the indirect effect in No_EMISS_NE compared to Only_EMISS_NE,
249 while moisture increase was much greater in No_EMISS_NE compared to Only_EMISS_NE due to a higher
250 direct + semi-direct effect.



251

252 Figure 4: Perturbation of EPT (K) due to total aerosol effect (Total), direct + semi-direct (D+S) and indirect (I) aerosol effect
253 in No_EMISS_NE (non-dashed), Only_EMISS_NE (dashed) and NOR-I (dashdot)

254 Moreover, the positive NE India regional average difference of column integrated cloud condensation
255 nuclei (CCN) number ($4.38 \times 10^{10} \text{ m}^{-2}$), cloud droplet number ($4.42 \times 10^{13} \text{ m}^{-2}$) and cloudwater (27.93 g m^{-2}), and
256 estimated from No_EMISS_NE – Only_EMISS_NE indicated that transported aerosols had a greater impact
257 through aerosol indirect effect (Zhang et al., 2010). The presence of larger aerosol amounts in the form of CCN
258 affects the cloud lifetime by affecting the conversion from cloudwater to rainwater, thus, to rainfall, thereby
259 suppressing rainfall, also known as the 2nd indirect effect (Shiogama et al., 2010; Cherian et al., 2017). Due to
260 more aerosol mass over NE India (Sect. 3.1), NOR-I and No_EMISS_NE had significantly higher cloudwater
261 compared to



262

263 Figure 5: NE India regional average vertical profiles of cloudwater mixing ratio (non-dashed) and rainwater mixing ratio
264 (dashed) in different scenarios (g kg^{-1})

265 Only_EMISS_NE, as seen in Fig. 5. Consequently, NOR-I and No_EMISS_NE had a significantly lower
266 rainwater mixing ratio than Only_EMISS_NE. Thus, rainfall suppression due to indirect effect was highest in
267 NOR-I, followed by No_EMISS_NE and Only_EMISS_NE. Hence, the combined effect of reduction in moisture,
268 instability and rainfall formation contributed to the reduction in rainfall through indirect and total aerosol effects.
269 This could be a possible key mechanism associated with the decreasing rainfall trend in the region. Reduction of
270 moisture due to the direct effect of aerosols and evaporation of clouds by BC were found to be possible
271 mechanisms by Barman and Gokhale (2022). However, this study shows that the contribution of direct and semi-
272 direct effects was very small compared to the indirect effect. The indirect effect has been found to be the dominant
273 aerosol effect in many studies (Wang et al., 2015; Liu et al., 2016) and was found to suppress monsoon rainfall
274 over India (Manoj et al., 2012). Aerosol indirect effect is mainly dictated by the warm clouds (Christensen et al.,
275 2016). Thus, the higher cloud cover associated with NOR-I and No_EMISS_NE in lower atmosphere which
276 affected SW radiation more in Sect. 3.2, was due to a greater amount of cloudwater in lower atmosphere.

277 Moreover, No_EMISS_NE and Only_EMISS_NE simulations were evaluated against the IMD rainfall
278 dataset and NOR-I simulation to check whether the local or transported aerosols had greater control over the



279 rainfall in NE India. No_EMISS_NE showed better regional average rainfall statistics than Only_EMISS_NE
280 with higher IOA (0.48 vs. 0.47), lower RMSE (18.85 vs. 20.37 mm day⁻¹), and lower ME (6.94 vs. 8.22 mm day⁻¹)
281 ¹) on comparing with the IMD rainfall dataset. Also, the simulated rainfall of No_EMISS_NE showed higher
282 rainfall similarity with NOR-I than Only_EMISS_NE with higher IOA (0.65 vs. 0.63), lower RMSE (56.32 vs.
283 61.92 mm day⁻¹) and lower ME (39.30 vs. 39.81 mm day⁻¹). Hence, No_EMISS_NE showed more similarity with
284 the baseline scenario as well as observed data and had greater control over the region's rainfall.

285 3.4 Role of local and transported BC

286 In section 3.3, the direct effect showed to increase moisture over NE India through an increase in atmospheric
287 instability, caused mainly due to atmospheric heating of BC (Barman and Gokhale (2022)) Hence, to negate the
288 effects of the indirect effect on atmospheric dynamics, scenarios in Table 1 containing only direct and semi-direct
289 effects were used in this analysis. Moreover, NOR gave a much better performance with BC concentration
290 estimation (Table S2) than when the indirect effect was included (NOR-I). The results from No_EMISS_NE,
291 Only_EMISS_NE, No_NE_BCI and Only_NE_BCI scenarios were compared and related.

292 3.4.1 Radiative heating

293 The regional average vertical profiles of NOR, 2NOR, No_NE_BC, No_NE_2×BC, Only_NE_BC and
294 Only_NE_2×BC can be seen from Fig. S5, in which the transported BC and local BC profiles resemble the
295 No_EMISS_NE and Only_EMISS_NE PM₁₀ profiles, respectively. IGP was the dominant source of transported
296 BC (Fig. S6). In transported BC scenarios, BC was available up to much higher atmospheric height and profiles
297 showed elevated concentration at around 1500 m indicating stronger BC transport at that height. In Only_NE_BC
298 and Only_NE_2×BC, BC was confined near the surface, which decreased continuously. The atmospheric heating
299 rate (HR) was estimated as per Liou (1980).

$$300 \quad HR = \frac{g}{C_p} \cdot \frac{\Delta F}{\Delta P}, \quad (4)$$

301 where g is the acceleration due to gravity (9.81 m s⁻²), C_p is the specific heat capacity of air at constant pressure
302 (1.005 kJ K⁻¹ kg⁻¹), ΔF the atmospheric RF and ΔP is the atmospheric pressure (300 hPa) difference between
303 surface and 3 km altitude as most of the BC was present below this height. Moreover, in order to compare the
304 effectiveness of heating by local and transported BC, two parameters, heating efficiency (HE) and heating slope
305 (HS), were defined by equations 5 and 6.

$$306 \quad HE = \frac{HR}{\text{Column sum of BC concentration within 3 km (CC)}}, \quad (5)$$

$$307 \quad HS = \frac{\Delta HR}{\Delta CC}, \quad (6)$$

308 HE has units of K day⁻¹ μg⁻¹ m³, thus measuring the heating contributed by per unit concentration of BC below 3
309 km. HE was used to assess the effect of BC vertical distribution on atmospheric heating while HS was used to
310 assess the response of atmospheric heating rate to BC concentration changes and has similar units as HE. CC has
311 units of μg m⁻³.

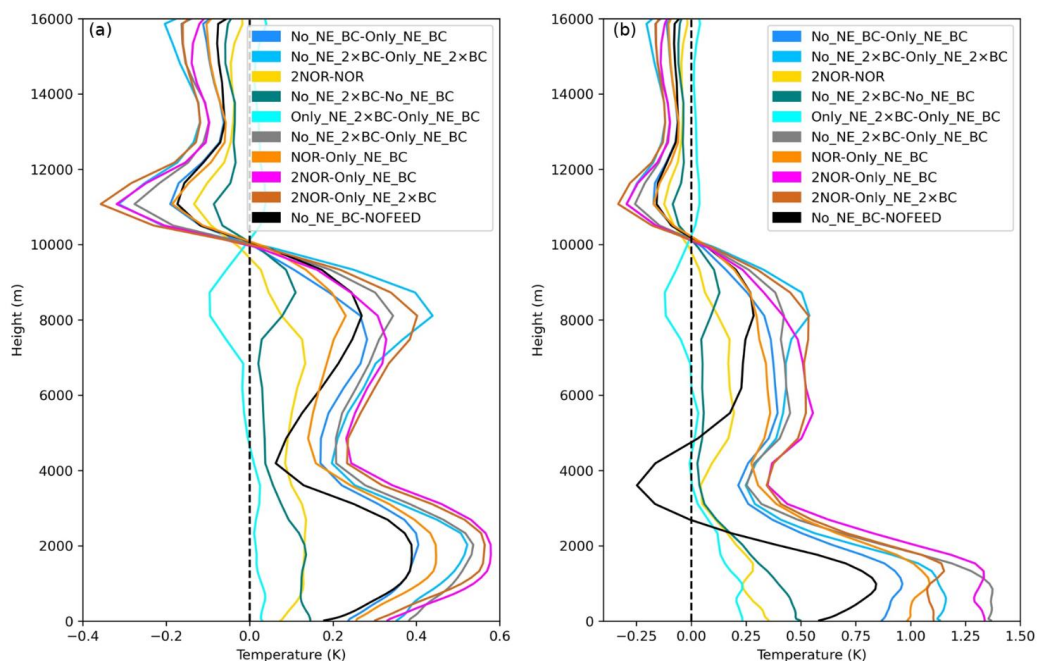


312 Table 3: NE India region average values of columnar BC concentration ($\mu\text{g m}^{-3}$) and atmospheric heating
313 parameters in different scenarios

	No_NE_BC	No_NE_2×BC	Only_NE_BC	Only_NE_2×BC
HR	0.460	0.597	0.123	0.178
CC	12.458	18.391	3.905	7.563
HE	0.037	0.032	0.032	0.024
ΔHE		-0.004		-0.008
HS		0.023		0.015

314 The quantitative values of the parameters are provided in Table 3. Only_NE_BC had a regional net average HR
315 of 0.123 K day^{-1} compared to 0.460 K day^{-1} of No_NE_BC. This indicated a 3.73 times higher atmospheric heating
316 rate by transported BC. An increase in local emissions from Only_NE_BC to Only_NE_2×BC caused a small
317 increase in heating rate of 0.055 K day^{-1} compared to the increase of 0.137 K day^{-1} from No_NE_BC to
318 No_NE_2×BC. As per the definition, HE was inversely proportional to CC and this was exactly followed in all
319 regions across all scenarios (Fig. S7 and S8). However, HE was higher in the case of transported BC compared to
320 local BC with values of $0.037 \text{ K day}^{-1} \mu\text{g}^{-1} \text{ m}^3$ (No_NE_BC) vs. $0.032 \text{ K day}^{-1} \mu\text{g}^{-1} \text{ m}^3$ (Only_NE_BC) and 0.032
321 $\text{K day}^{-1} \mu\text{g}^{-1} \text{ m}^3$ (No_NE_2×BC) vs. $0.024 \text{ K day}^{-1} \mu\text{g}^{-1} \text{ m}^3$ (Only_NE_2×BC), even if CC was higher in the case
322 of transported BC. The reason might be that transported BC might have undergone a higher amount of chemical
323 transformation due to higher atmospheric time, leading to a higher lensing effect on the BC core, resulting in
324 enhanced absorption (Liu et al., 2015). Also, it was observed that on increasing emissions, the decrease in HE was
325 smaller in the case of transported BC ($-0.004 \text{ K day}^{-1} \mu\text{g}^{-1} \text{ m}^3$) than local BC ($-0.008 \text{ K day}^{-1} \mu\text{g}^{-1} \text{ m}^3$). Hence, with
326 the increase in BC emissions, HE decreased more when BC was more concentrated near the surface than in the
327 atmosphere. HS indicated that atmospheric heating increased at a higher rate of $0.023 \text{ K day}^{-1} \mu\text{g}^{-1} \text{ m}^3$ with
328 increasing transported BC compared to $0.015 \text{ K day}^{-1} \mu\text{g}^{-1} \text{ m}^3$. Thus, the increase in transported BC emissions had
329 more impact on atmospheric heating over NE India than when present near the surface with local emissions.

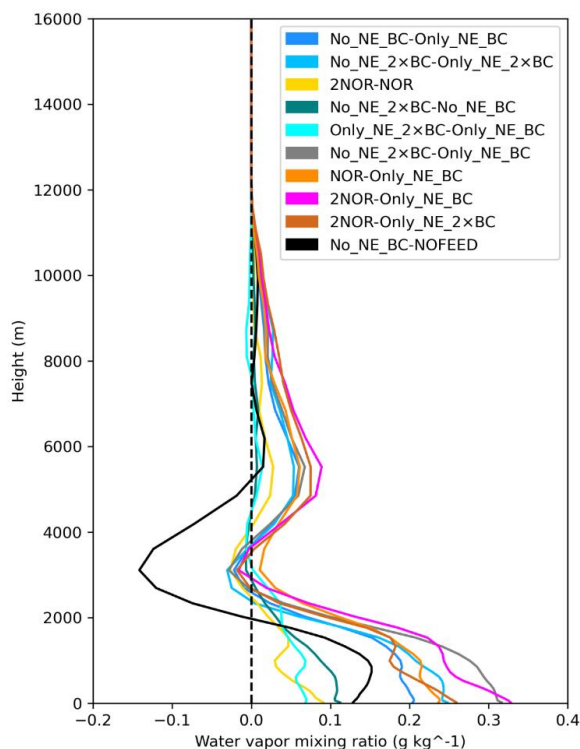
330 3.4.2 Atmospheric stability and moisture



331

332 Figure 6: Regionally averaged vertical profiles showing perturbations in a) potential temperature b) equivalent
333 potential temperature

334 Barman and Gokhale (2022), as well as Soni et al. (2017), showed an increased influx of moisture into the region
335 during pre-monsoon due to BC. In order to compare and separate the effects of local and transported BC on
336 atmospheric stability through temperature and moisture, potential temperature (PT) and EPT were estimated. PT
337 estimates atmospheric stability based on temperature, while EPT accounts for both temperature and moisture and
338 is a more realistic parameter. In most of the profiles in both parameters in Fig. 6(a) and 6(b), positive perturbation
339 was observed approximately below 10 km and negative above it which indicated an increase in atmospheric
340 instability and vice-versa for an increase in atmospheric stability. (Zhao et al., 2011). The positive perturbations
341 below 10 km varied with height and were most profound in the profiles No_NE_BC – Only_NE_BC,
342 No_NE_2xBC – Only_NE_2xBC and No_NE_2xBC – Only_NE_BC, each of which was estimated from the
343 difference between a transported BC scenario and local BC scenario. These profiles showed similarity with the
344 corresponding profiles of NOR – Only_NE_BC, 2NOR – Only_NE_2xBC and 2NOR – Only_NE_BC in both
345 the parameters, indicating that they were closer to the normal atmospheric scenario. The positive perturbations
346 were, however, comparatively smaller with 2NOR – NOR, No_NE_2xBC – No_NE_BC and Only_NE_2xBC –
347 Only_NE_BC in both the parameters, each pair being the same scenario with only a difference in emission rates.
348 This shows that BC atmospheric distribution played an important role on instability. The Only_NE_2xBC –
349 Only_NE_BC profile not only showed a smaller increase in instability than No_NE_2xBC – No_NE_BC profile
350 but also contributed to the smallest increase in instability in both the parameters. Thus, transported BC and an
351 increase in transported BC emissions led to higher atmospheric instability than local BC.



352

353 Figure 7: Regionally averaged vertical profiles showing perturbations in water vapor mixing ratio (g kg^{-1})

354 Moreover, EPT profiles showed higher positive perturbations and hence higher instability compared to
355 the corresponding PT profiles with values exceeding 1.25 K. The positive difference or additional instability
356 between the corresponding profiles of Fig. 6(a) and 6(b) was due to moisture. The difference also indicated that
357 moisture contributed even more to the instability than BC. The peaks for EPT existed closer to the surface due to
358 most of the moisture also remaining near the surface, as shown in Fig. 7. However, there occurred a region of
359 increased stability from the ground surface to the first peak of transported BC profiles at approximately 1000 m,
360 indicated by increasing temperature with height. Thus, transported BC may also be responsible for air quality
361 scenarios over NE India by creating a stable boundary layer. The close qualitative and quantitative similarity
362 between No_NE_BC – NOFEED, No_NE_BC – Only_NE_BC and NOR – Only_NE_BC profiles in Fig. 6(a)
363 showed that aerosol radiative effect due to transported BC was intricately linked with the PT profile and the
364 positive perturbations in each of these profiles were also closely linked with BC. This was also seen in Fig. 6(b),
365 but since it also included the effect of moisture, larger differences were seen.

366 BC, whether transported or emitted locally, caused a positive perturbation in moisture at least below 2
367 km altitude, as seen in Fig. 7. The perturbation was much larger in profiles that had a combination of transported
368 and local BC scenarios and which had higher transported BC emissions and followed the pattern similar to PT
369 and EPT. This links BC, instability and moisture in the region, i.e., higher transported BC caused higher instability
370 which brought a higher amount of moisture which would possibly again cause higher instability. It was the same



371 for scenarios that included indirect effect, as can be observed from the similarities of the No_NE_BCI –
372 Only_NE_BCI (Fig. S9) and No_NE_BC – Only_NE_BC profile in Fig.7. Furthermore, the similarity of
373 No_EMISS_NE – Only_EMISS_NE profile with No_NE_BCI – Only_NE_BCI (Fig. S9) inferred that direct
374 radiative effect of transported BC was responsible for the moisture increase in Fig. 3. The higher moisture with
375 transported BC scenarios was due to higher moisture flux caused by it over Bay of Bengal compared to local BC
376 and can be verified from Fig. S10. Quantitatively, No_NE_BC (33.95 kg m^{-2}) and No_NE_2×BC (34.15 kg m^{-2})
377 had higher region average precipitable water vapor than Only_NE_BC (33.49 kg m^{-2}) and Only_NE_2×BC (33.64
378 kg m^{-2}). Hence transported BC in Sect. 3.3 was primarily responsible for transporting moisture from the Bay of
379 Bengal by affecting the atmospheric dynamics. The mechanism is similar to the "heat pump" model by Lau et al.
380 (2006).

381 3.5 Rainfall response to emissions

382 Similar to NOR-I – NOCHEM, No_BC_ABS – NOCHEM gave the rainfall change due to total aerosol effect,
383 but without BC absorption. The higher negative rainfall change of -275.13 mm with NOR-I – NOCHEM
384 compared to -266.78 mm with No_BC_ABS – NOCHEM showed BC absorption to reduce rainfall. The higher
385 reduction with NOR-I – NOCHEM was mainly due to higher rainfall reduction in region 1, where the direct and
386 semi-direct effect was maximum. This shows BC initially suppressed rainfall even though moisture increased due
387 to it. However, with the increase in BC emissions, rainfall increased and the rainfall suppression due to the total
388 aerosol effect reduced substantially to -64.44 mm with 4NOR-I – NOCHEM compared to -275.13 mm with NOR-
389 I – NOCHEM and similarly, rainfall due to direct and semi-direct with 4NOR-I – NOFEED-I showed a positive
390 rainfall change of 193.64 mm compared to -17.04 mm with NOR-I – NOFEED. Similarly, 4NOR-I – NOR-I gave
391 a rainfall enhancement of 225.24 mm. Aged BC also contributes as CCN (Lambe et al., 2015). The enhancement
392 in BC emission did increase the column average CCN concentration to 2252 m^{-3} (4NOR-I) from 2024 m^{-3} (NOR-
393 I), but the increase was largely disproportionate to the 4 times BC emission increase. However, in spite of the
394 increase in CCN, cloudwater mixing ratio was lower in 4NOR-I than NOR-I, as seen in Fig. 5 and 4NOR-I caused
395 significantly more rainfall formation than NOR-I, as can be seen from the rainwater mixing ratio profiles. This
396 may be related to the suppression of CCN activation due to BC, as observed over Central India (Nair Jayachandran
397 et al., 2020). Also BC contributes marginally to indirect effect (Kristjánsson, 2002). Thus, the increased moisture
398 (Fig. S9) did not remain stored as cloudwater even though there was an increase in CCN, but it got converted to
399 rainwater. This indicated that the increase in BC emissions didn't contribute to rainfall suppression through
400 indirect aerosol effect though there was an increase in CCN concentration, but rather counteracted the suppression
401 of rainfall due to the indirect effect of other aerosol species. The rainfall enhancement was due to an increase in
402 moisture, contributed by the transported fraction of BC, as explained in Sect. 3.4.2. Moreover, rainfall suppression
403 was also more due to transported aerosols, mainly contributed by indirect effect (Table 2).

404 Also, among the non-absorbing aerosols, sulfate aerosol is an important contributor to CCN and indirect
405 effect (Kristjánsson, 2002). Its concentration was found to be the highest among non-absorbing aerosols and most
406 of its mass over NE India was found to be transported (Sect. 3.1). Concentration profiles can be seen from Fig.
407 S11. Hence, the response of rainfall over NE India was checked by increasing (No_EMISS_NE_4SO₂) and
408 decreasing (No_EMISS_NE_0.25SO₂) SO₂ emissions outside NE India and compared against the baseline
409 transported scenario (No_EMISS_NE) since sulfate is mainly formed within the atmosphere by oxidation of SO₂



410 (Wang et al., 2021). Similar to the increase in BC emissions, No_EMISS_NE_4SO₂ caused an increase in column
411 average CCN concentration to 3524 m⁻³ compared to 1753 m⁻³ in No_EMISS_NE, while
412 No_EMISS_NE_0.25SO₂ showed a decrease (1390 m⁻³). However, contrary to the BC, an increase in SO₂
413 emissions with No_EMISS_NE_4SO₂ caused an increase in cloudwater mixing ratio compared to
414 No_EMISS_NE, as seen in Fig. 5, while its decrease also caused a decrease. Thus, No_EMISS_NE_4SO₂ and
415 No_EMISS_NE_0.25SO₂ had lower and higher rainwater mixing ratio, respectively, compared to
416 No_EMISS_NE. Consequently, No_EMISS_NE_4SO₂ had higher rainfall suppression and gave lesser rainfall (-
417 22.23 mm) compared to No_EMISS_NE_0.25SO₂. Thus, an increase in non-absorbing aerosol caused rainfall
418 suppression through indirect effect. The indirect effect was observed to be the dominant aerosol effect for
419 suppressing rainfall. However, with an increase in BC, suppression of rainfall due to direct and semi-direct effects
420 through surface processes (surface moisture flux, convection) and cloud evaporation as well as due to indirect
421 aerosol effect (atmospheric stability, surface moisture flux and cloud to rainwater conversion) becomes
422 comparatively weaker mechanisms than the direct effect of radiative heating by BC, enhancing rainfall through
423 the transport of moisture. However, the increase in transported SO₂ emissions also caused further suppression of
424 rainfall. Hence, an increase in transported aerosols of an absorbing aerosol (BC) and a non-absorbing aerosol
425 (sulfate), both being a contributor to CCN, showed different responses to indirect effect parameters and thus to
426 rainfall and hence most likely controls the enhancement and suppression of pre-monsoon rainfall over NE India,
427 thus counteracting each other. However, since decreasing rainfall trend has been observed, the impacts of the
428 indirect aerosol effect could be dominant. Here, the response of only one non-absorbing aerosol (sulfate) was
429 checked and possibly has contributions from other similar species also.

430 Moreover, the percentage of the simulation time different aerosol effects and BC emissions increased
431 (inc) or suppressed (dec) rainfall under different rainfall intensities (low: 0-5, medium: 5-10, high: > 10 mm day⁻¹;
432 defined as per (Raju et al., 2015)) and the rainfall amount under those intensities was estimated. Regional
433 average values are provided in Table S5 and S6. All aerosol effects caused a higher decrease across all rainfall
434 intensities, except the indirect effect, which indicated a higher increase in low-intensity rainfall (6.52 mm vs. -
435 6.48 mm; 21.44 % vs. 20.58 %). High-intensity rain was primarily responsible for rainfall changes across all the
436 scenarios and effects. The indirect effect decreased high-intensity rainfall duration (18.85 vs. 12.38 %) and amount
437 (-399.41 mm vs. 141.62 mm) and was primarily responsible for the rainfall suppression in total aerosol effect (-
438 411.34 mm). The total aerosol effect with enhanced BC emissions (4NOR-I – NOCHEM) showed a significantly
439 higher increase (275.47 mm vs. 137.16 mm) as well as a significantly lower decrease (-337.23 vs. -411.34) in
440 high-intensity rainfall compared to total aerosol effect with baseline BC emissions (NOR-I – NOCHEM). Similar
441 results in time and rainfall amount between BC increase and direct + semi-direct effect with BC increase scenarios
442 inferred that enhanced radiative effects due to BC increase were mainly responsible for higher high-intensity
443 rainfall duration and rainfall amount, while the indirect aerosol effect was mainly involved in its suppression,
444 possibly due to the increased atmospheric stability associated with it. Barman and Gokhale (2022) also showed
445 similar results with BC emissions increase, but this study verifies the role of direct radiative effects of BC in it.
446 Thus, BC increased rainfall over NE India but in the form of high-intensity rainfall. Hence, relative fractions of
447 BC and the other aerosols contributing to indirect effect possibly decide the amount of rainfall and its intensity
448 over the region. However, indirect effect also caused high-intensity rainfall but with lesser amount than its
449 suppression and may be involved in catastrophic flood events at local scales (Wang et al., 2022).



450 **4 Conclusions**

451 Transported aerosols, primarily from IGP, were found to be responsible for the bulk of the aerosol mass (93.98
452 %) over NE India while contributing 64.18 % of near-surface PM₁₀ concentration, thus primarily responsible for
453 air pollution as climatic impacts over the region during pre-monsoon season. The climatic impacts, both w.r.t. RF
454 as well as rainfall, were dominated by the indirect aerosol effect. The impacts of the indirect aerosol effects of
455 transported aerosols were much higher in affecting radiation (-13.12 W m⁻² vs. -0.24 W m⁻² at the surface, 7.30 W
456 m⁻² vs. 0.97 W m⁻² in the atmosphere) as well as suppressing rainfall (-49.11 mm vs. -16.04 mm) compared to
457 local emissions. The greater surface dimming by transported aerosols caused a higher negative change in surface
458 moisture flux (-3.82×10⁻⁶ kg m⁻² s⁻¹ vs. 8.15×10⁻⁸ kg m⁻² s⁻¹) as well as higher aerosol mass reduced cloudwater to
459 rainwater conversion, both of which contributed to higher rainfall suppression. Transported aerosols caused
460 4.42×10¹³ m⁻² higher cloud droplets than local emissions. The atmospheric instability due to the direct + semi-
461 direct effect and indirect effect of transported aerosols were found to be contradictory and caused an increase and
462 decrease, respectively. The direct effect of transported aerosols, though also caused negative surface moisture flux
463 over NE India (-1.03×10⁻⁶ kg m⁻² s⁻¹), however, increased moisture over NE India, increasing moisture flux over
464 the Bay of Bengal. Further analysis showed that transported BC was more efficient in atmospheric heating over
465 NE India and together with the higher transported BC mass, an increase in its emissions caused higher atmospheric
466 instability over the region, which brought more moisture from the Bay of Bengal. The increased moisture further
467 contributed to higher instability. Hence, the rainfall suppression caused through the different atmospheric
468 processes by direct, semi-direct and indirect effects was reduced and nullified with the increase in BC emissions,
469 but the rainfall increase was mainly in the form of high-intensity rainfall. The increase in BC did not show a
470 positive change in cloudwater, though it contributed to CCN. The direct effect of BC thus overpowered the other
471 rainfall-suppressing processes. Indirect aerosol effect and radiative heating were the main rainfall-controlling
472 factors. Hence, changes in emissions of aerosols or chemical species contributing to these processes will possibly
473 contribute to rainfall suppression and enhancement over NE India. Moreover, rainfall simulated with transported
474 aerosols were found to be more similar to the IMD observation datasets as well as the baseline emission scenario,
475 indicating its possible greater influence in the real-world scenario.

476 The study shows that the atmospheric transport of emissions from IGP to NE India has a significant
477 impact on NE India's atmosphere during pre-monsoon and the impacts are even greater than the emissions within
478 the NE India region.

479 **Data availability.** Model outputs are available upon request.

480 **Author contributions.** NB - conceptualization, methodology, model simulation, visualisation, manuscript
481 writing, SG - conceptualization, methodology and supervision, manuscript review and editing.

482 **Competing interests.** The authors declare that they have no conflict of interest.

483 **Disclaimer.** The views expressed in this paper are those of the authors.

484 **Acknowledgements.** The simulations were performed on the "Param-Ishan" HPC of Indian Institute of
485 Technology Guwahati. The authors are also grateful to "Air and Noise Pollution Lab" of Civil Department IIT
486 Guwahati for their support.

487 **References**

488 Bagtasa, G., Cayetano, M. G., Yuan, C. S., Uchino, O., Sakai, T., Izumi, T., Morino, I., Nagai, T., Macatangay,
489 R. C., and Velasco, V. A.: Long-range transport of aerosols from East and Southeast Asia to northern



- 490 Philippines and its direct radiative forcing effect, *Atmos. Environ.*, 218, 117007,
491 <https://doi.org/10.1016/j.atmosenv.2019.117007>, 2019.
- 492 Barman, N. and Gokhale, S.: Urban black carbon - source apportionment, emissions and long-range transport
493 over the Brahmaputra River Valley, *Sci. Total Environ.*, 693, 1–14,
494 <https://doi.org/10.1016/j.scitotenv.2019.07.383>, 2019.
- 495 Barman, N. and Gokhale, S.: Aerosol influence on the pre-monsoon rainfall mechanisms over North-East India:
496 A WRF-Chem study, *Atmos. Res.*, 268, 106002, <https://doi.org/10.1016/j.atmosres.2021.106002>, 2022.
- 497 Bauer, S. E. and Menon, S.: Aerosol direct, indirect, semidirect, and surface albedo effects from sector
498 contributions based on the IPCC AR5 emissions for preindustrial and present-day conditions,
499 <https://doi.org/10.1029/2011JD016816>, 2012.
- 500 Bhat, M. A., Romshoo, S. A., and Beig, G.: Characteristics, source apportionment and long-range transport of
501 black carbon at a high-altitude urban centre in the Kashmir valley, North-western Himalaya, *Environ. Pollut.*,
502 305, 119295, <https://doi.org/10.1016/j.envpol.2022.119295>, 2022.
- 503 Bollasina, M. A., Ming, Y., and Ramaswamy, V.: Anthropogenic aerosols and the weakening of the south asian
504 summer monsoon, *Science* (80-.), 334, 502–505, <https://doi.org/10.1126/science.1204994>, 2011.
- 505 Bonasoni, P., Laj, P., Marinoni, A., Sprenger, M., Angelini, F., Arduini, J., Bonafè, U., Calzolari, F., Colombo,
506 T., Decesari, S., Di Biagio, C., Di Sarra, A. G., Evangelisti, F., Duchi, R., Facchini, M. C., Fuzzi, S., Gobbi, G.,
507 P., Maione, M., Panday, A., Roccatò, F., Sellegri, K., Venzac, H., Verza, G. P., Villani, P., Vuillermoz, E., and
508 Cristofanelli, P.: Atmospheric Brown Clouds in the Himalayas: First two years of continuous observations at the
509 Nepal Climate Observatory-Pyramid (5079 m), *Atmos. Chem. Phys.*, 10, 7515–7531,
510 <https://doi.org/10.5194/acp-10-7515-2010>, 2010.
- 511 Bond, T. C., Doherty, S. J., Fahey, D. W., Forster, P. M., Berntsen, T., Deangelo, B. J., Flanner, M. G., Ghan,
512 S., Kärcher, B., Koch, D., Kinne, S., Kondo, Y., Quinn, P. K., Sarofim, M. C., Schultz, M. G., Schulz, M.,
513 Venkataraman, C., Zhang, H., Zhang, S., Bellouin, N., Guttikunda, S. K., Hopke, P. K., Jacobson, M. Z., Kaiser,
514 J. W., Klimont, Z., Lohmann, U., Schwarz, J. P., Shindell, D., Storelvmo, T., Warren, S. G., and Zender, C. S.:
515 Bounding the role of black carbon in the climate system: A scientific assessment, *J. Geophys. Res. Atmos.*, 118,
516 5380–5552, <https://doi.org/10.1002/jgrd.50171>, 2013.
- 517 Chatterjee, A., Adak, A., Singh, A. K., Srivastava, M. K., Ghosh, S. K., Tiwari, S., Devara, P. C. S., and Raha,
518 S.: Aerosol chemistry over a high altitude station at northeastern Himalayas, India, *PLoS One*, 5,
519 <https://doi.org/10.1371/journal.pone.0011122>, 2010.
- 520 Chaudhury, A. S., Nikhil, V. A., and Gokhale, S.: Black carbon in different climatic seasons of the Brahmaputra
521 River Valley of Northeast India – Field measurements at two different heights and analysis, *Atmos. Pollut. Res.*,
522 13, 101327, <https://doi.org/10.1016/j.apr.2022.101327>, 2022.
- 523 Cherian, R., Quaas, J., Salzmann, M., and Tomassini, L.: Black carbon indirect radiative effects in a climate
524 model, *Tellus, Ser. B Chem. Phys. Meteorol.*, 69, 1–10, <https://doi.org/10.1080/16000889.2017.1369342>, 2017.
- 525 Christensen, M. W., Chen, Y. C., and Stephens, G. L.: Aerosol indirect effect dictated by liquid clouds, *J.*
526 *Geophys. Res.*, 121, 14636–14650, <https://doi.org/10.1002/2016JD025245>, 2016.
- 527 Dahutia, P., Pathak, B., and Bhuyan, P. K.: Aerosols characteristics, trends and their climatic implications over
528 northeast india and adjoining South Asia, *Int. J. Climatol.*, 38, 1234–1256, <https://doi.org/10.1002/joc.5240>,
529 2018.
- 530 Dahutia, P., Pathak, B., and Bhuyan, P. K.: Vertical distribution of aerosols and clouds over north-eastern South
531 Asia: Aerosol-cloud interactions, *Atmos. Environ.*, 215, 116882,
532 <https://doi.org/10.1016/j.atmosenv.2019.116882>, 2019.
- 533 Emery, C., Tai, E., and Yarwood, G.: Enhanced Meteorological Modeling and Performance Evaluation for Two
534 Texas Ozone Episodes, *Env. Int. Corp.*, 235, 2001.
- 535 Ghan, S. J., Liu, X., Easter, R. C., Zaveri, R., Rasch, P. J., Yoon, J. H., and Eaton, B.: Toward a minimal
536 representation of aerosols in climate models: Comparative decomposition of aerosol direct, semidirect, and
537 indirect radiative forcing, *J. Clim.*, 25, 6461–6476, <https://doi.org/10.1175/JCLI-D-11-00650.1>, 2012.
- 538 Gogoi, M. M., Babu, S. S., Moorthy, K. K., Bhuyan, P. K., Pathak, B., Subba, T., Chutia, L., Kundu, S. S.,



- 539 Bharali, C., Borgohain, A., Guha, A., Kumar De, B., Singh, B., and Chin, M.: Radiative effects of absorbing
540 aerosols over northeastern India: Observations and model simulations, *J. Geophys. Res.*, 122, 1132–1157,
541 <https://doi.org/10.1002/2016JD025592>, 2017.
- 542 Grell, G. A., Peckham, S. E., Schmitz, R., McKeen, S. A., Frost, G., Skamarock, W. C., and Eder, B.: Fully
543 coupled “online” chemistry within the WRF model, *Atmos. Environ.*, 39, 6957–6975,
544 <https://doi.org/10.1016/j.atmosenv.2005.04.027>, 2005.
- 545 Guha, A., De, B. K., Dhar, P., Banik, T., Chakraborty, M., Roy, R., Choudhury, A., Gogoi, M. M., Babu, S. S.,
546 and Moorthy, K. K.: Seasonal Characteristics of Aerosol Black Carbon in Relation to Long Range Transport
547 over Tripura in Northeast India, 786–798, <https://doi.org/10.4209/aaqr.2014.02.0029>, 2015.
- 548 Habib, G., Venkataraman, C., Chiapello, I., Ramachandran, S., Boucher, O., and Shekar Reddy, M.: Seasonal
549 and interannual variability in absorbing aerosols over India derived from TOMS: Relationship to regional
550 meteorology and emissions, *Atmos. Environ.*, 40, 1909–1921, <https://doi.org/10.1016/j.atmosenv.2005.07.077>,
551 2006.
- 552 Kant, S., Panda, J., Rao, P., Sarangi, C., and Ghude, S. D.: Study of aerosol-cloud-precipitation-meteorology
553 interaction during a distinct weather event over the Indian region using WRF-Chem, *Atmos. Res.*, 247,
554 <https://doi.org/10.1016/j.atmosres.2020.105144>, 2021.
- 555 Kedia, S., Cherian, R., Islam, S., Das, S. K., and Kaginalkar, A.: Regional simulation of aerosol radiative effects
556 and their influence on rainfall over India using WRFChem model, *Atmos. Res.*, 182, 232–242,
557 <https://doi.org/10.1016/j.atmosres.2016.07.008>, 2016.
- 558 Kedia, S., Das, S. K., Islam, S., Hazra, A., and Kumar, N.: Aerosols impact on the convective and non-
559 convective rain distribution over the Indian region: Results from WRF-Chem simulation, *Atmos. Environ.*, 202,
560 64–74, <https://doi.org/10.1016/j.atmosenv.2019.01.020>, 2019.
- 561 Koch, D. and Del Genio, A. D.: Black carbon semi-direct effects on cloud cover: Review and synthesis, *Atmos.*
562 *Chem. Phys.*, 10, 7685–7696, <https://doi.org/10.5194/acp-10-7685-2010>, 2010a.
- 563 Koch, D. and Del Genio, A. D.: Black carbon semi-direct effects on cloud cover: Review and synthesis, *Atmos.*
564 *Chem. Phys.*, 10, 7685–7696, <https://doi.org/10.5194/acp-10-7685-2010>, 2010b.
- 565 Krishnamohan, K. S., Modak, A., and Bala, G.: Effects of local and remote black carbon aerosols on summer
566 monsoon precipitation over india, *Environ. Res. Commun.*, 3, <https://doi.org/10.1088/2515-7620/AC18D1>,
567 2021.
- 568 Kristjánsson, J. E.: Studies of the aerosol indirect effect from sulfate and black carbon aerosols, *J. Geophys.*
569 *Res. Atmos.*, 107, 1–19, <https://doi.org/https://doi.org/10.1029/2001JD000887>, 2002.
- 570 Kumar, M., Parmar, K. S., Kumar, D. B., Mhawish, A., Broday, D. M., Mall, R. K., and Banerjee, T.: Long-
571 term aerosol climatology over Indo-Gangetic Plain: Trend, prediction and potential source fields, *Atmos.*
572 *Environ.*, 180, 37–50, <https://doi.org/10.1016/j.atmosenv.2018.02.027>, 2018.
- 573 Kundu, S. S., Borgohain, A., Barman, N., Devi, M., and Raju, P. L. N.: Spatial Variability and Radiative Impact
574 of Aerosol along the Brahmaputra River Valley in India: Results from a Campaign, *J. Environ. Prot. (Irvine,*
575 *Calif.)*, 09, 405–430, <https://doi.org/10.4236/jep.2018.94026>, 2018.
- 576 Lambe, A. T., Ahern, A. T., Wright, J. P., Croasdale, D. R., Davidovits, P., and Onasch, T. B.: Oxidative aging
577 and cloud condensation nuclei activation of laboratory combustion soot, *J. Aerosol Sci.*, 79, 31–39,
578 <https://doi.org/10.1016/j.jaerosci.2014.10.001>, 2015.
- 579 Lau, K. M., Kim, M. K., and Kim, K. M.: Asian summer monsoon anomalies induced by aerosol direct forcing:
580 The role of the Tibetan Plateau, *Clim. Dyn.*, 26, 855–864, <https://doi.org/10.1007/s00382-006-0114-z>, 2006.
- 581 Lee, H. J., Jo, Y. J., Kim, S., Kim, D., Kim, J. M., Choi, D., Jo, H. Y., Bak, J., Park, S. Y., Jeon, W., and Kim,
582 C. H.: Transboundary aerosol transport process and its impact on aerosol-radiation-cloud feedbacks in
583 springtime over Northeast Asia, *Sci. Rep.*, 12, 1–10, <https://doi.org/10.1038/s41598-022-08854-1>, 2022.
- 584 Liou, K. N.: *An Introduction to Atmospheric Radiation*, 1980.
- 585 Liu, S., Aiken, A. C., Gorkowski, K., Dubey, M. K., Cappa, C. D., Williams, L. R., Herndon, S. C., Massoli, P.,
586 Fortner, E. C., Chhabra, P. S., Brooks, W. A., Onasch, T. B., Jayne, J. T., Worsnop, D. R., China, S., Sharma,



- 587 N., Mazzoleni, C., Xu, L., Ng, N. L., Liu, D., Allan, J. D., Lee, J. D., Fleming, Z. L., Mohr, C., Zotter, P.,
588 Szidat, S., and Prévôt, A. S. H.: Enhanced light absorption by mixed source black and brown carbon particles in
589 UK winter, *Nat. Commun.*, 6, <https://doi.org/10.1038/ncomms9435>, 2015.
- 590 Liu, X. Y., Zhang, Y., Zhang, Q., and He, K. Bin: Application of online-coupled WRF/Chem-MADRID in East
591 Asia: Model evaluation and climatic effects of anthropogenic aerosols, *Atmos. Environ.*, 124, 321–336,
592 <https://doi.org/10.1016/j.atmosenv.2015.03.052>, 2016.
- 593 Lohmann, U. and Feichter, J.: Can the direct and semi-direct aerosol effect compete with the indirect effect on a
594 global scale?, *Geophys. Res. Lett.*, 28, 159–161, <https://doi.org/10.1029/2000GL012051>, 2001.
- 595 Manoj, M. G., Devara, P. C. S., Joseph, S., and Sahai, A. K.: Aerosol indirect effect during the aberrant Indian
596 Summer Monsoon breaks of 2009, *Atmos. Environ.*, 60, 153–163,
597 <https://doi.org/10.1016/j.atmosenv.2012.06.007>, 2012.
- 598 Menon, S., Hansen, J., Nazarenko, L., and Luo, Y.: Climate effects of black carbon aerosols in China and India,
599 *Science (80-.)*, 297, 2250–2253, <https://doi.org/10.1126/science.1075159>, 2002.
- 600 Mitchell, J. M.: The Effect of Atmospheric Aerosols on Climate with Special Reference to Temperature near the
601 Earth's Surface, [https://doi.org/10.1175/1520-0450\(1971\)010<0703:teoao>2.0.co;2](https://doi.org/10.1175/1520-0450(1971)010<0703:teoao>2.0.co;2), 1971.
- 602 Mondal, A., Lakshmi, V., and Hashemi, H.: Intercomparison of trend analysis of Multisatellite Monthly
603 Precipitation Products and Gauge Measurements for River Basins of India, *J. Hydrol.*, 565, 779–790,
604 <https://doi.org/10.1016/j.jhydrol.2018.08.083>, 2018.
- 605 Nair Jayachandran, V., Nair Suresh Babu, S., Vaishya, A., Gogoi, M. M., Nair, V. S., Krishnakumari Sathesh,
606 S., and Krishna Moorthy, K.: Altitude profiles of cloud condensation nuclei characteristics across the Indo-
607 Gangetic Plain prior to the onset of the Indian summer monsoon, *Atmos. Chem. Phys.*, 20, 561–576,
608 <https://doi.org/10.5194/acp-20-561-2020>, 2020.
- 609 Nair, V. S., Babu, S. S., Manoj, M. R., Moorthy, K. K., and Chin, M.: Direct radiative effects of aerosols over
610 South Asia from observations and modeling, *Clim. Dyn.*, 49, 1411–1428, <https://doi.org/10.1007/s00382-016-3384-0>, 2017.
- 612 Nandan, R., Ratnam, M. V., Kiran, V. R., and Naik, D. N.: Aerosol-cloud interaction in water clouds observed
613 using ground-based, in-situ, and satellite-based observations over an Indian continental region, *Atmos. Res.*,
614 280, 106436, <https://doi.org/10.1016/j.atmosres.2022.106436>, 2022.
- 615 Nenes, A., Conant, W. C., and Seinfeld, J. H.: Black carbon radiative heating effects on cloud microphysics and
616 implications for the aerosol indirect effect 2. Cloud microphysics, *J. Geophys. Res. Atmos.*, 107, AAC 24-1-
617 AAC 24-11, <https://doi.org/10.1029/2002jd002101>, 2002.
- 618 Ojha, N., Naja, M., Singh, K. P., Sarangi, T., Kumar, R., Lal, S., Lawrence, M. G., Butler, T. M., and Chandola,
619 H. C.: Variabilities in ozone at a semi-urban site in the Indo-Gangetic Plain region: Association with the
620 meteorology and regional processes, *J. Geophys. Res. Atmos.*, 117, 1–19,
621 <https://doi.org/10.1029/2012JD017716>, 2012.
- 622 Ojha, N., Sharma, A., Kumar, M., Girach, I., Ansari, T. U., Sharma, S. K., Singh, N., Pozzer, A., and Gunthe, S.
623 S.: On the widespread enhancement in fine particulate matter across the Indo-Gangetic Plain towards winter,
624 *Sci. Rep.*, 10, 1–9, <https://doi.org/10.1038/s41598-020-62710-8>, 2020.
- 625 Pai, D. S., Sridhar, L., Rajeevan, M., Sreejith, O. P., Satbhai, N. S., and Mukhopadhyay, B.: Development of a
626 new high spatial resolution ($0.25^\circ \times 0.25^\circ$) long period (1901-2010) daily gridded rainfall data set over India
627 and its comparison with existing data sets over the region, *Mausam*, 65, 1–18, 2014.
- 628 Pathak, B., Kalita, G., Bhuyan, K., Bhuyan, P. K., and Moorthy, K. K.: Aerosol temporal characteristics and its
629 impact on shortwave radiative forcing at a location in the northeast of India, 115, 1–14,
630 <https://doi.org/10.1029/2009JD013462>, 2010.
- 631 Pathak, B., Subba, T., Dahutia, P., Bhuyan, P. K., Moorthy, K. K., Gogoi, M. M., Babu, S. S., Chutia, L., Ajay,
632 P., Biswas, J., Bharali, C., Borgohain, A., Dhar, P., Guha, A., De, B. K., Banik, T., Chakraborty, M., Kundu, S.
633 S., Sudhakar, S., and Singh, S. B.: Aerosol characteristics in north-east India using ARFINET spectral optical
634 depth measurements, *Atmos. Environ.*, 125, 461–473, <https://doi.org/10.1016/j.atmosenv.2015.07.038>, 2016.
- 635 Raju, A., Parekh, A., Chowdary, J. S., and Gnanaseelan, C.: Assessment of the Indian summer monsoon in the



- 636 WRF regional climate model, *Clim. Dyn.*, 44, 3077–3100, <https://doi.org/10.1007/s00382-014-2295-1>, 2015.
- 637 Ramanathan, V., Chung, C., Kim, D., Bettge, T., Buja, L., Kiehl, J. T., Washington, W. M., Fu, Q., Sikka, D. R.,
638 and Wild, M.: Atmospheric brown clouds: Impacts on South Asian climate and hydrological cycle, *Proc. Natl.*
639 *Acad. Sci.*, 102, 5326–5333, <https://doi.org/10.1073/pnas.0500656102>, 2005.
- 640 Rana, A., Jia, S., and Sarkar, S.: Black carbon aerosol in India: A comprehensive review of current status and
641 future prospects, *Atmos. Res.*, 218, 207–230, <https://doi.org/10.1016/j.atmosres.2018.12.002>, 2019.
- 642 Rosenfeld, D.: Suppression of rain and snow by urban air pollution, *Science (80-.)*, 287, 1793–1796,
643 <https://doi.org/10.1126/science.287.5459.1793>, 2012.
- 644 Sarangi, C., Tripathi, S. N., Tripathi, S., and Barth, M. C.: Aerosol-cloud associations over gangetic basin
645 during a typical monsoon depression event using WRF-Chem simulation, *J. Geophys. Res.*, 120, 10,974–10,995,
646 <https://doi.org/10.1002/2015JD023634>, 2015.
- 647 Sarkar, C., Roy, A., Chatterjee, A., Ghosh, S. K., and Raha, S.: Factors controlling the long-term (2009–2015)
648 trend of PM 2.5 and black carbon aerosols at eastern Himalaya, India, *Sci. Total Environ.*, 656, 280–296,
649 <https://doi.org/10.1016/j.scitotenv.2018.11.367>, 2019.
- 650 Shiogama, H., Emori, S., Takahashi, K., Ogura, T. N., Nozawa, T., and Takemura, T.: Emission scenario
651 dependency of precipitation on global warming in the MIROC3.2 model, *J. Clim.*, 23, 2404–2417,
652 <https://doi.org/10.1175/2009JCLI3428.1>, 2010.
- 653 Singh, S. and Gokhale, S.: Source apportionment and light absorption properties of black and brown carbon
654 aerosols in the Brahmaputra River valley region, *Urban Clim.*, 39, 100963,
655 <https://doi.org/10.1016/j.uclim.2021.100963>, 2021.
- 656 Soni, P., Tripathi, S. N., and Srivastava, R.: Radiative effects of black carbon aerosols on Indian monsoon: a
657 study using WRF-Chem model, *Theor. Appl. Climatol.*, 132, 115–134, <https://doi.org/10.1007/s00704-017-2057-1>, 2017.
- 659 Talukdar, S., Venkat Ratnam, M., Ravikiran, V., and Chakraborty, R.: Influence of Black Carbon Aerosol on the
660 Atmospheric Instability, *J. Geophys. Res. Atmos.*, 124, 5539–5554, <https://doi.org/10.1029/2018JD029611>,
661 2019.
- 662 Tiwari, S., Kumar, R., Tunved, P., Singh, S., and Panicker, A. S.: Significant cooling effect on the surface due
663 to soot particles over Brahmaputra River Valley region, India: An impact on regional climate, *Sci. Total*
664 *Environ.*, 562, 504–516, <https://doi.org/10.1016/j.scitotenv.2016.03.157>, 2016.
- 665 Tripathi, S. N., Dey, S., Tare, V., and Sathesh, S. K.: Aerosol black carbon radiative forcing at an industrial
666 city in northern India, *Geophys. Res. Lett.*, 32, 1–4, <https://doi.org/10.1029/2005GL022515>, 2005.
- 667 Twomey, S.: The influence of pollution on the shortwave albedo of clouds, *J. Atmos. Sci.*, 1149–1152117,
668 [https://doi.org/doi.org/10.1175/1520-0469\(1977\)034<1149:TlOPOT>2.0.CO;2](https://doi.org/doi.org/10.1175/1520-0469(1977)034<1149:TlOPOT>2.0.CO;2), 1977.
- 669 Wang, K., Zhang, Y., Yahya, K., Wu, S. Y., and Grell, G.: Implementation and initial application of new
670 chemistry-aerosol options in WRF/Chem for simulating secondary organic aerosols and aerosol indirect effects
671 for regional air quality, *Atmos. Environ.*, 115, 716–732, <https://doi.org/10.1016/j.atmosenv.2014.12.007>, 2015.
- 672 Wang, K., Hattori, S., Lin, M., Ishino, S., Alexander, B., Kamezaki, K., Yoshida, N., and Kang, S.: Isotopic
673 constraints on atmospheric sulfate formation pathways in the Mt. Everest region, southern Tibetan Plateau,
674 *Atmos. Chem. Phys.*, 21, 8357–8376, <https://doi.org/10.5194/acp-21-8357-2021>, 2021.
- 675 Wang, Y., Zheng, X., Dong, X., Xi, B., Wu, P., Logan, T., and Yung, Y. L.: Impacts of long-range transport of
676 aerosols on marine-boundary-layer clouds in the eastern North Atlantic, *Atmos. Chem. Phys.*, 20, 14741–14755,
677 <https://doi.org/10.5194/acp-20-14741-2020>, 2020.
- 678 Wang, Z., Xue, L., Liu, J., Ding, K., Lou, S., Ding, A., Wang, J., and Huang, X.: Roles of Atmospheric
679 Aerosols in Extreme Meteorological Events: a Systematic Review, *Curr. Pollut. Reports*, 8, 177–188,
680 <https://doi.org/10.1007/s40726-022-00216-9>, 2022.
- 681 Yang, Q., Gustafson, W. I., Fast, J. D., Wang, H., Easter, R. C., Morrison, H., Lee, Y. N., Chapman, E. G.,
682 Spak, S. N., and Mena-Carrasco, M. A.: Assessing regional scale predictions of aerosols, marine stratocumulus,
683 and their interactions during VOCALS-REx using WRF-Chem, *Atmos. Chem. Phys.*, 11, 11951–11975,



- 684 <https://doi.org/10.5194/acp-11-11951-2011>, 2011.
- 685 Zhang, Y., Wen, X. Y., and Jang, C. J.: Simulating chemistry-aerosol-cloud-radiation-climate feedbacks over
686 the continental U.S. using the online-coupled Weather Research Forecasting Model with chemistry
687 (WRF/Chem), *Atmos. Environ.*, 44, 3568–3582, <https://doi.org/10.1016/j.atmosenv.2010.05.056>, 2010.
- 688 Zhao, C., Liu, X., Leung, L. R., and Hagos, S.: Radiative impact of mineral dust on monsoon precipitation
689 variability over West Africa, *Atmos. Chem. Phys.*, 11, 1879–1893, <https://doi.org/10.5194/acp-11-1879-2011>,
690 2011.
- 691
- 692
- 693